Enhanced ionic conductivity with Li7O2Br3 phase in Li3OBr anti-perovskite solid electrolyte

ZHU, JINLONG
LI, SHUAI
ZHANG, YI
HOWARD, JOHN
Lu, Xujie
WANG, YONGGANG
Kummar, Ravih
WANG, LIPING
ZHAO, YUSHENG

To be published in: Applied Physics Letters

DOI to publisher's version: 10.1063/1.4962437

Enhanced ionic conductivity with $Li_7O_2Br_3$ phase in Li_3OBr anti-perovskite solid electrolyte

Jinlong Zhu[1†*], Shuai Li[1†], Yi Zhang[1], John W. Howard[1], Xujie Lü[2], Yonggang Wang[1], Ravih S. Kummar[1], Liping Wang[1], Yusheng Zhao[1*]

[1]High Pressure Science and Engineering Center, University of Nevada, Las Vegas, Nevada 89154, United States

[2]Center for Integrated Nanotechnologies and Earth and Environmental Sciences Division, Los Alamos National Laboratory, Los Alamos, NM 87545, United States

Abstract:

Cubic Anti-perovskite with general formula Li_3OX (X = Cl, Br, I) was recently reported as superionic conductors for solid electrolyte of all-solid-state lithium ion batteries. The materials are nonflammable, low-cost and suitable for thermoplastic processing. However, the obstacle of its practical application is harmed by the relatively low ionic conductivity at room temperature. In this work, we synthesized the two phase mixing compound of Li_3OBr and $Li_7O_2Br_3$ by solid state reaction routes. The results indicated that with the weigh ratio of $Li_7O_2Br_3$ increasing, the ionic conductivity was enhanced by more than one order of magnitude compared with pure phase Li_3OBr. Theoretical calculation showed that $Li_7O_2Br_3$ is a meta-stable phase, which results in no single phase $Li_7O_2Br_3$ obtained. High pressure technique or chemical methods could change the kinetic route of $Li_7O_2Br_3$ formation.

Keywords: solid electrolyte, lithium ion battery, Lithium-rich Anti-Perovskite, layered structure

[†]Authors contributed equally to this work

[*]To whom correspondence should be addressed. Jinlong Zhu: jlzhu04@physics.unlv.edu; Yusheng Zhao: yusheng.zhao@unlv.edu

1. Introduction

Lithium ion batteries (LIBs) are critical for energy storage especially for their wide application in electric vehicles and portable devices [1-4]. Currently, using liquid electrolytes are the most obstruction for transport energy storage as their toxic, corrosive and flammable [5,6]. So the rapid developed solid state electrolytes are expected to conquer all the drawbacks and lead to a safety and environmental friendly applications [7-10]. Furthermore, another advantage of using solid electrolytes in LIBs is no lithium dendrite formed [11] while using lithium metal as the anode, which can enhance the energy/power density. Never the less, solid electrolyte needs to surpass or at least similar to the parameters as in liquid electrolytes, such as high ionic conductivity, low conducting activation energy, negligible electronic conductivity, large electrochemical, and compatible with electrodes [8]. Currently, there are few reported solid electrolytes with good performances. [12-16]. For instance, the newly developed lithium superionic conductor $Li_{10}GeP_2S_{12}$, with a new three-dimensional framework, has a Li^+ conductivity of 1.2×10^{-2} S/cm at room temperature, which is the highest ionic conductivity reported of solid electrolyte [15]. The garnet-type $Li_7La_3ZrO_{12}$ has high bulk ionic conductivity but huge grain boundary resistance [13,14]. Nanoporous β-Li_3PS_4 was reported to have conductivity of 1.6×10^{-4} S/cm at room temperature [16]. NASICON [13] and LISICON [17,18] compounds are widely studied solid state fast lithium conductors these decades. However, there is no solid electrolyte for now can fulfill all the requirements of replacing liquid electrolytes in LIBs.

Exploration of new class solid electrolyte can not only enhance the flexibility of full solid-state battery design, and also can contribute to the requirements of portable energy storage and transportation in a environmental friendly and safer way. The recent reported antiperovskite electrolyte family [19,20], evolved from perovskite of $NaMgF_3$ and (K,Na)MgF_3, could be a promising system as the results of perovskite structure tolerance and Li^+ superionic conductor. The advantage of Li3OA (A = halogens) is the large electrochemical window, low electronic conductivity [21,22] and stable with lithium metal anode [23]. The relatively low ionic conductivity needs to be further enhanced by structural manipulations, such as doping, Li^+ depleting.

In this work, we demonstrated a layered structural $Li_7O_2Br_3$ compound, which is thermal dynamically unstable compared with Li_3OBr, was kinetically quenched as a mixing phase while Li_3OBr was synthesized. We found that with the percentage increasing of $Li_7O_2Br_3$ in the mixing phase, the ionic conductivity slowly increased and the active energy decreased. After the weight percentage reached up to ~ 40%, there is a turning point and the trends exacerbate. At the mixing phase with maximum $Li_7O_2Br_3$ weight percentage we can get, the ionic conductivity at room temperature reached to 0.24×10^{-4} S/cm.

2. Experimental methods

Pure phase cubic antiperovskite of Li_3OBr and mixing phase of Li_3OBr and $Li_7O_2Br_3$ have been synthesized by solid state reaction inside the glovebox with starting materials of Li_2O (Alfa Aesar, 99.5 %) and LiBr (Alfa Aesar, anhydrous, 99 %) fine powders. Briefly, the reaction is under the protection of inert gas with oxygen level and moisture level all less than 10 ppm; the materials were weighted in mole ratios, mixed and grinded inside glovebox. The mixed raw materials were loaded in crucibles. The solid reaction occurred at 480 °C for 16 hours for at least three times with ball milling for 1 hour. For ball milling process, the raw materials were loaded into sealed ball milling jars inside glovebox and then transferred to ball milling machine. The basic reaction pathway is shown in **Equation (1)** and **(2)**:

$$Li_2O + LiBr \rightarrow Li_3OBr \quad \textbf{(1)}$$

$$2Li_2O + 3LiBr \rightarrow Li_7O_2Br_3 \quad \textbf{(2)}$$

The X-ray powder diffraction (XRD) patterns were recorded on an X-ray diffractometer (Bruker D8 Advance). The as synthesized powders sealed in a zero background air tight sample holder. The crystal parameters and phase ratio were analyzed by the Rietveld refinements by using GSAS+EXPGUI software package [24].

Electrochemical impedance spectra (EIS) were measured inside the glovebox of sample synthesis. The samples were melted in between two pieces of Au foil electrodes forming symmetric cells. The cells were kept for 1 hour after reaching the targeted temperature in the furnace at each setting point before impedance measurement. Solartron 1260A instrument was used for the EIS measurement with applied AC voltage of 10 mV in the frequency range from 1 MHz to 1 Hz.

The crystal structures of Li_3OBr, LiBr and Li_7O_2Br from refinement were employed as the initial structure model to study the total energy as a function of cell volume. The the stability calculation for $Li_7O_2Br_3$ were performed by using CASTEP software [25] at the GGA level of theory and energy cutoff of 380 eV, by consider the reaction: $2*(Li_3OBr)+LiBr=Li_7O_2Br_3$.

3. Results and Discussion

As reported and shown in Figure 1, Li_3OBr crystallizes into the cubic antiperovskite structure with space group of *Pm*-3*m* and with a = 4.0347(6) Å comprising of corner-sharing OLi_6 octahedrons and Br^- anions located in A-site [26]; and the layered $Li_7O_2Br_3$ is tetragonal antiperovskite with space group of *I*4/*mmm*, a = 4.0148(5) Å and c = 21.4811(5) Å, and the refined parameters are listed in Table 1.

According to the theoretical calculation, both Li_3OBr [27] and $Li_7O_2Br_3$ are meta-stable phase compared with the starting Li_2O and LiBr materials. Furthermore, $Li_7O_2Br_3$ is even unstable than Li_3OBr phase. The calculated total energy of Li_3OBr + LiBr mixture is -22.49957 meV lower than $Li_7O_2Br_3$ per formula unit. It indicates that the layered $Li_7O_2Br_3$ could be meta-stable relative to Li_3OBr since LiBr is a very stable compound. Therefore, it could be a little difficult to synthesize $Li_7O_2Br_3$ without competing phase mixture like Li_3OBr-LiBr or Li_2O-LiBr. However, by kinetic process control both phases can be quenched to room temperature. Figure 1 gives a represent diffraction pattern with 44 w% $Li_7O_2Br_3$. For current effort, the maximum weight percentage of $Li_7O_2Br_3$ in the two-phase mixing composite is up to 44 w%, as shown in Figure 2. For all the reactions, there are un-reacted or decomposed Li_2O and LiBr in the final products, as indicated in Figure 1 and 2. Because the phase purity has influence on the ionic conductivity, the comparison of the three composites with 39 w%, 41 w% and 44 w% $Li_7O_2Br_3$ indicated the sudden increase of the ionic conductivity is the intrinsic property other than from the impurities.

Figure 3 gives all the impendence measurements of mixing phase samples from room temperature to 180 ºC. In Figure 3 (f), the typical impedance spectra of Li_3OBr at room temperature consists two semi-circles, the high frequency one from bulk resistance, and low frequency one from grain boundary. It is clear that the grain boundary resistance dominates the total resistance. It should be noticed that as the emerging of the layered $Li_7O_2Br_3$ in the samples, the grain boundary contributions to the ionic conductivities (as the second semi-cycle in pure Li_3OBr sample in Figure 3 (a) and (f)) vanished, indicating the existing of $Li_7O_2Br_3$ phase also improve the grain boundary conductivities. All the EIS data were fitted by equivalent circuit and the bulk ionic conductivities were plotted in Figure 4 (a). Figure 4 (b) gives the ionic conductivities as the function of $Li_7O_2Br_3$ phase weight percentage at room temperature (RT). The ionic conductivity at RT changed from 10^{-6} S/cm for Li_3OBr (consistence with reported in Ref [27]) to 0.24×10^{-4} S/cm for mixing phase sample with 44 w% $Li_7O_2Br_3$, more than an order of magnitude increase. In the temperature range studied, the conductivities of all the samples follow the Arrhenius equation, and the derived active energy E_a was plotted in Figure 4 (c). It is interesting to find that with the $Li_7O_2Br_3$ weight percentage increasing in the mixing phase samples, the ionic conductivity increased slowly and active energy decreased slowly until there is turning point at the weight percentage of 40 %. After that, the ionic conductivity increased rapidly and correspondingly the active energy decreased suddenly. It is well established the ionic conductivity transport pathway is along the edge of the octahedron, either O^{2-} in perovskite [28] or Li^+ in antiperovskite [21]. The stoichiometric crystal lattice is not good Li^+ conductors [22]. However, in the layered $Li_7O_2Br_3$ structure, the insolated octahedral polyhedrons (as shown in the inset of Figure 1) gives the possibilities of creating more Li^+ defects and vacancies to enhance the ionic conductivity. Based on experimental results in Figure 4, we suspected that the fast Li ionic transport pathway connected while the $Li_7O_2Br_3$ weight percentage reaching to 40%, resulting in the rapid increase of ionic conductivity. Further efforts of making pure phase $Li_7O_2Br_3$ sample is being explored by tradition solid state reaction, pulse laser deposition and high pressure methods.

4. Conclusions

In this work, pure phase Li_3OBr, as well as its phase mixing composites with $Li_7O_2Br_3$ was synthesized via solid state reaction. $Li_7O_2Br_3$ is a meta-stable phase from theoretical calculation. Its promising high ionic conductivity makes it worthy of experimental pure phase acquisition and Li ionic transport mechanism exploration by TEM or neutron diffractions.

Acknowledgments

The authors are grateful for the financial support by the ARPA-E project (0670-3052).

References:

[1]. M. Armand, J. M. Tarascon, *Nature* **451** (2008) 652.

[2]. R. Marom, S.F. Amalraj, N. Leifer, D. Jacob, D. Aurbach, *J. Mater. Chem.* **21** (2011) 9938.

[3]. M. Wakihara, *Mat. Sci. Eng.* **R33** (2001) 109.

[4]. J. M. Tarascon, M.Armand, *Nature* **414** (42001) 359.

[5]. A. Patil, V. Patil, D. W. Shin, J. W. Choi, D. S. Paik, S. J. Yoon, *Mater. Res. Bull.* **43** (2008) 1913.

[6]. J. B. Goodenough, Y. Kim, *Chem. Mater.* **22** (2010) 587.

[7]. J. B. Goodenough, K.S. Park, *J. Am. Chem. Soc.* **135** (2013) 1167.

[8]. E. Quartarone, P. Mustarelli, *Chem. Soc. Rev.* **40** (2011) 2525.

[9]. H. Lee, M. Yanilmaz, O. Toprakci, K. Fu, X.W. Zhang, *Energ. Environ. Sci.* **7** (2014) 3857.

[10]. V. Etacheri, R. Marom, R. Elazari, G. Salitra, D. Aurbach, *Energ. Enviro. Sci.* **4** (2011) 3243.

[11]. W. Xu.; J. L. Wang, F. Ding, X. L. Chen, E. Nasybutin, Y. H. Zhang, J.G. Zhang, *Energ. Environ. Sci.* **7** (2014) 513.

[12]. J. T. Han, J. L. Zhu, Y. T. Li, X. H. Yu, S. M. Wang, G. Wu, H. Xie, S. C. Vogel, F. Izumi, K. Momma, Y. Kawamura, Y. H. Huang, J. B. Goodenough, Y.S. Zhao, *Chem. Commun.* **48** (2012) 9840.

[13]. J. B. Goodenough, H. Y. P. Hong, J. A. Kafalas, *Mater. Res. Bull.* **11** (1976) 203.

[14]. R. Murugan, V. Thangadurai, W. Weppner, *Angew. Chem. Int. Ed.* **46** (2007) 7778.

[15]. N. Kamaya, K. Homma, Y. Yamakawa, M. Hirayama, R. Kanno, M. Yonemura, T. Kamiyama, Y. Kato, S. Hama, K. Kawamoto, A. Mitsui, *Nat. Mater.* **10** (2011) 682.

[16]. Z. C. Liu, W. J. Fu, E. A. Payzant, X. Yu, Z. L. Wu, N. J. Dudney, J. Kiggans, K .L. Hong, A. J. Rondinone, C.D. Liang, *J. Am. Chem. Soc.* **135** (2013) 975.

[17]. P. G. Bruce, A.R. West, *J. Electrochem. Soc.* **130** (1983) 662.

[18]. H. Y. P. Hong, *Mater. Res. Bull.* **13** (1978) 117.

[19]. Y. Zhao and L. L. Daemen, *J. Am. Chem. Soc.*, 2012, **134**, 15042-15047.

[20]. Y. Wang, Q. Wang, Z. Liu, Z. Zhou, S. Li, J. Zhu, R. Zou, Y. Wang, J. Lin and Y. Zhao, *J. Power Sources*, 2015, **293**, 735-740.

[21]. A. Emly, E. Kioupakis, A. Van der Ven, *Chem. Mater.* **25** (2013) 4663.

[22]. Y. Zhang, Y. S. Zhao, C. F. Chen, *Phys. Rev. B* **87** (2013) 134303.

[23]. X. J. Lu, G. Wu, J. W. Howard, A. P. Chen, Y. S. Zhao, L. L. Daemen, Q. X. Jia, *Chem. Commun.* **50** (2014) 11520.

[24]. A. C. Larson and R. B. Von Dreele, *Los Alamos National Laboratory Report* 2004, LAUR 86-748.

[25]. OLD. J. Clark, M. D. Segall, C. J. Pickard, P. J. Hasnip, M. J. Probert, K. Refson and M. C. Payne, *Z. Kristallogr.* **200** (2005) 567.

[26]. K. Hippler, S. Sitta, P. Vogt and H. Sabrowsky, *Acta Cryst.*, 1990, **C46**, 736-738.

[27]. S. Li, J. L. Zhu, Y. G. Wang, J. W. Howard, X. J. Lü, Y. T. Li, R. S. Kumar, L. P. Wang, L. L. Daemen, Y. S. Zhao, *Solid State Ionics* **284** (2016) 14–19.

[28]. Perovskite Oxide for Solid Oxide Fuel Cells, Fuel cell and hydrogen energy, I. Tatsumi (Ed.) Springer Science+Business Media LLC, New York 2009, ISBN: 978-0-387-77707-8.

Figure and table captions:

Table 1 Refined crystal parameters for Li_3OBr and $Li_7O_2Br_3$ at room temperature; the occupancy for all the atoms and the thermal parameters for all Li atoms were fixed during the refinement.

Figure 1 Powder X-ray diffraction pattern of mixing phase of Li_3OBr and $Li_7O_2Br_3$; the empty black circles and solid red lines are from experiment and refinement. The blue tricks correspond to the indexing of cubic Li_3OBr with space group *Pm*-3*m*; and the red tricks correspond to the peak positions of layered $Li_7O_2Br_3$ with space group *I*4*/mmm*. Peaks marked by solid circle and by diamond are from LiBr and Li_2O respectively. The insets give the schematic show of the cubic and layered antiperovskite structures, and the green, brown and red balls (in the center of the octahedrons) represent the Li, Br and O atoms, respectively.

Figure 2 X-ray diffraction patterns of pure cubic phase Li3OBr and with mixing phase of Li_7O_2Br weight percentage up to 44 w%.

Figure 3 Impendence measurement of pure Li_3OBr (a) and two phase mixing samples (b-e); (f) The impedance spectrum of Li_3OBr at 25 ^oC, and equivalent circuit fitting result.

Figure 4 (a) Arrhenius plot of the bulke conductivity of mixing phase of Li_3OBr and $Li_7O_2Br_3$ between 25 ^oC and 180 ^oC with Au foil as electrodes; the activation energy E_a is derived by linear fitting of $\ln(\sigma T)$ versus 1/T. (b)-(c) give the ionic conductivities and active energies as a function of $Li_7O_2Br_3$ weight percentage in the mixing phase samples.

Table 1

Formula	Lattice parameters (Å)		Coordinates of equivalent positions: x	y	z	Occupancy	Thermal parameters (U_{iso})
Li_3OBr (56 w%)	a = **4.0347(6)**	Li	0.5	0	0	1.0	0.02
		O	0.5	0.5	0.5	1.0	0.02(2)
		Br	0	0	0	1.0	0.018(2)
$Li_7O_2Br_3$ (56 w%)	a = **4.0148(5)** c = **21.4811(5)**	Li1	0	0.5	0.093(2)	1.0	0.02
		Li2	0	0	0.1865(1)	1.0	0.02
		Li3	0	0	0	1.0	0.02
		Br1	0	0	0.3121(3)	1.0	0.02(1)
		Br2	0	0	0.5	1.0	0.02(1)
		O	0	0	0.09806(3)	1.0	0.03(1)

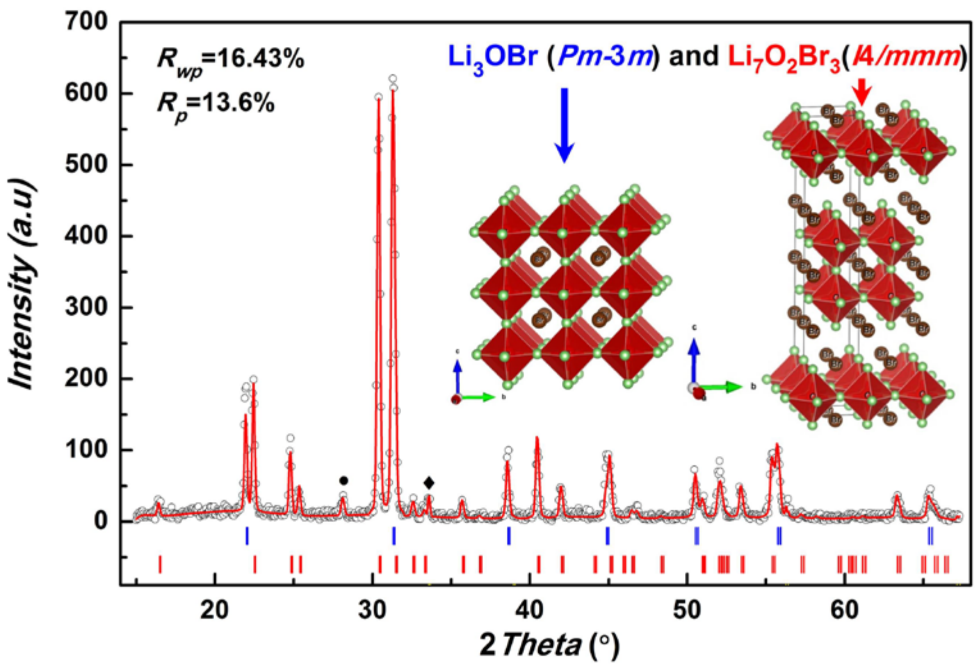

R_{wp}=16.43%
R_p=13.6%
Li_3OBr (*Pm-3m*) and $Li_7O_2Br_3$(*I4/mmm*)
Intensity (a.u)
2 *Theta* (°)

Figure 1

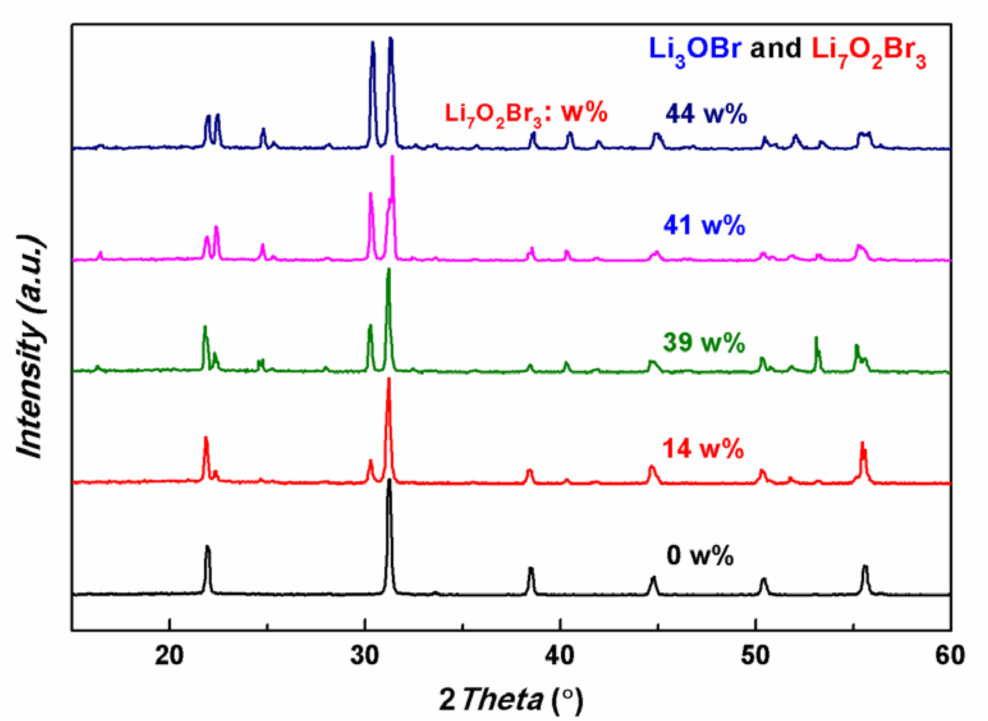
Li3OBr and Li7O2Br3
Li7O2Br3: w%
44 w%
41 w%
39 w%
14 w%
0 w%
Intensity (a.u.)
20
30
40
50
60
2 Theta (°)

Figure 2

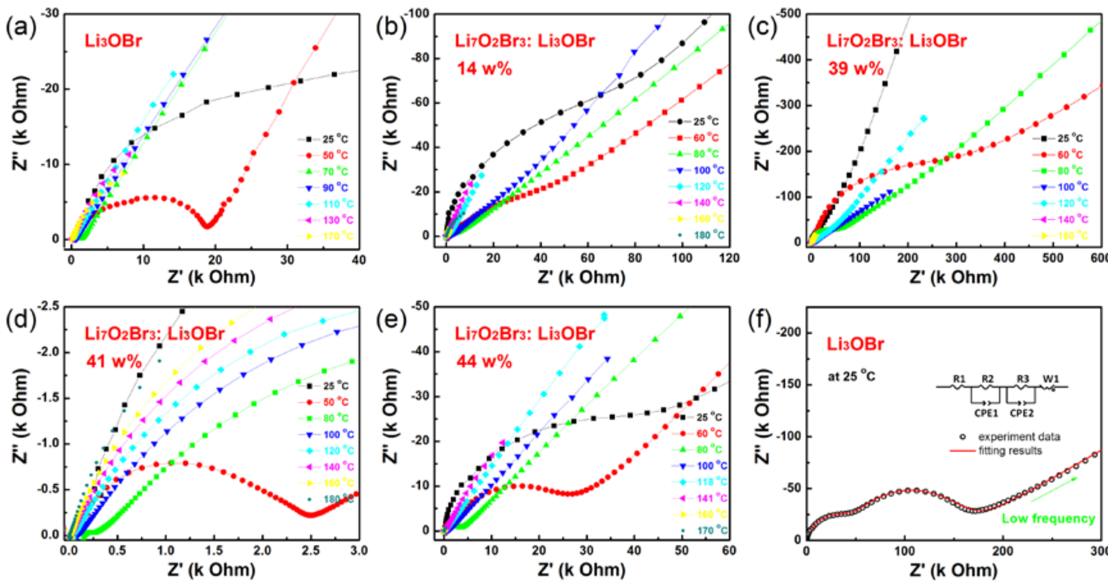

Figure 3

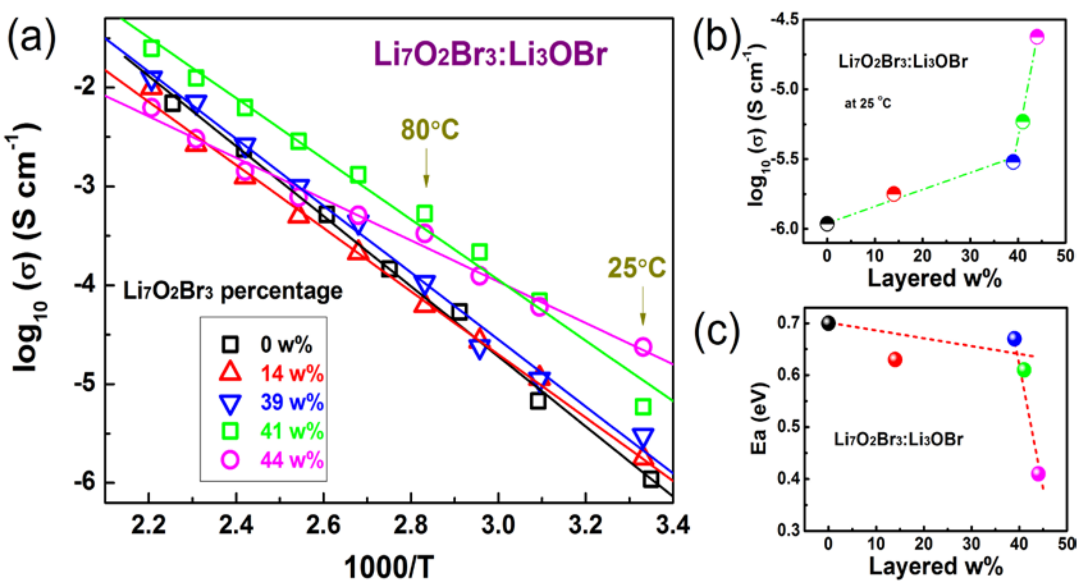
(a)
Li7O2Br3:Li3OBr
80°C
25°C
Li7O2Br3 percentage
0 w%
14 w%
39 w%
41 w%
44 w%
log10 (σ) (S cm-1)
1000/T
(b)
Li7O2Br3:Li3OBr
at 25 °C
Layered w%
(c)
Li7O2Br3:Li3OBr
Ea (eV)
Layered w%

Figure 4